Vortex and Oil Distribution of Oil-Water Annular Flow through Ball Valve

Fan, Jiang*[+]***; Sijie, Li; Oingfeng, Wu; Zhenzhang, Liu***

School of Mechanical and Electric Engineering, Guangzhou University, Guangzhou, 510006, P.R. CHINA

ABSTRACT: *The study on the flow behave inside of a ball valve is important for heavy crude oil transportation. Owe to the fast progress of the numerical technique, it becomes an effective way to observe the flows inside a valve and to analyze the flow structure of the oil-water core annular flow. In the present study, the simulation of the oil-water core annular flowing through the valve is conducted by combined the VOF and CSF model, and the effects of open rate on vortex and oil distribution characteristics are analyzed. The simulated data is a satisfactory match with empirical value and the experimental results. The results show that there are lots of vortexes inside and behind the valve, the coordinate values of the vortex decrease and the aggregation rate increases with increase in open rate. As the input velocity increases, the change rate of the vortex position is greater, and the oil aggregation rate decreases, the highly viscous oil with has greater aggregation rate after flow through the valve, and the variation of the vortex core position is relatively slow. As the vortex flow across the oil core, the oil will be scattered and contributes to the instability of the annular flow.*

KEYWORDS: *The ball valve; Oil-water annular flow; VOF; Vortex; Oil phase distribution; Numerical simulation.*

INTRODUCTION

An increase in the production of the heavy oil, the transport with core-annular flow is reliable and economic, in which the oil core is in the pipe center and the water flows between the oil core and the wall surface [1]. Many researchers observe the oil-water flow through the pipe. *Russell* and *Charles* [2] introduced the earliest experimental results and derived the theoretical prediction equations of pressure gradient. Then, the other researchers presented some experimental studies. *Charles et al.* [3] investigated oil water two phase flow of equal density in horizontal pipe, observed the flow patterns, and measured the pressure drops. *Arney et al.* [4] did the new experiments on the lubricated pipelining of crude oil, and built a correlation formula. *Grassi et al.* [5] conducted an experiment for flow-pattern and pressure drop in the horizontal and slightly inclined pipe. *Strazza et al.* [6] focused on the core-annular flow, measured pressure drop and oil hold-up, and compared the pressure gradients and hold-up data to the empirical correlation equations. These experiments are for horizontal core annular flow. *Bai et al.* [7] made experiments on water-lubricated flow in a vertical apparatus, and bamboo waves in upflow, corkscrew waves in downflow were observed. *Gabryk et al.* [8] measured hold-up during liquid-liquid

** To whom correspondence should be addressed.*
+ E-mail: jiangfan2008@gzhu.edu.cn
1021-9986/2019/2/239-252 14/$/6.04

flow through a vertical pipe. These are for the vertical annular flow. *Arney et al*. [4], *Grassi et al*. [5], *Rodriguez et al*. [9] obtained the numerous analytical models for estimating the existence range of core flow and pressure loss characteristics. At the same time, lots of studies have been presented to explain the hold conditions of the oil-water core annular flow. *Bentwich* [10] obtained the interface structure by considering gravity, interfacial tension, and capillary forces. *Howard et al*. [11] analyzed the linearized stability of the oil-water core annular flow in a horizontal pipe. And then, they [12] also studied the non-axisymmetric stability of core annular flow. *Azizi, et al.* [13] used the Probabilistic Neural Network (PNN) to prediction the flow pattern and oil holdup. These experiments and analyses are great value to analyze of the oil-water core annular flow, but that rarely considered core annular flow in complex flow path, such as a valve inner path during the opening and closing.

Due to numerical simulation with CFD technique can obtain much information on core annular flow, it becomes an important way to observe the flows inside a pipe and to analyze the stability of oil-water core annular flow. *Li* and *Renardy* [14] improved the wave simulation by using a VOF (volume of fluid) model and by setting at different density for two liquids. *Ooms et al.* [15] applied the VOF model for simulating the horizontal core flow with a density difference between the liquids to study the buoyancy effect to core annular flow. *Sumana et al.* [16] studied the lube oil-water core annular flow through U-bend, and obtained some characteristic about hydrodynamics and fouling by using the FLUENT system. *Jiang et al*. [17] compared the difference between VOF model and the Eulerian model by using the software FLUENT 14.5. They [18] also analyzed the water and non-Newtonian oil core annular flow through rectangle return bends. The VOF model is also used to simulate the free surface fluid flow, such as droplet dynamics prediction, bubble motion, and so on [19-20], on the other hand, not much is known about used in the complex flow path for the core annular flow.

The valves are common pipefitting, and largely used in engineering such as water supply and drainage, air conditioning, refrigeration, petrochemical industries, ventilation, and so on. During the last years, several analysises of the inner flow state of valves have conducted numerical simulation. *Xu et al.* [21] employed CFD codes to evaluate the flow inside of Contra-push check valve and discussed the steady characteristics. *Posa et al* [22] conducted a direct numerical simulation with an immersed-boundary method to analyze the hydraulic valve. *Valdes et al*. [23] performed a series of CFD simulations of the cavitation flow through a ball check valve. These studies indicate that CFD simulation is a valid tool to analyze flow behaviors inside the valve. However, the ball valve is one of the valves, and is important piping parts, as the core annular flow inside it, the flow is very complicated, and is no report about that. The valve has a ball with different open rates to control the flow rate, which may have different impacts on the hydrodynamics characteristics and flow structure.

The aim of this work is to analyze the oil-water flow behavior when it flows through ball valve and the effects of input water fraction, oil property, open rate on vortex and oil phase distribution. The relationship of vortex and aggregation rate of oil phase is tried to analyze too. The results may give the references for optimizing the operation parameters of the ball valve in the heavy oil transportation.

THEORITICAL SECTION

Description of governing equations

Two-phase Model

The numerical analysis method of multiphase flows has are two types: the Euler-Lagrange approach and the Euler-Euler approach. In the Euler-Euler method, there are three models for solving two-phase flow problems, which are the VOF model, the Mixture model, and the Eulerian model [24-27]. The VOF model is a numerical formulation for tracking interfaces of two fluids which are not inter-penetrating and is relatively simple and accurate [1], so it is considered in this study.

The VOF model includes the volume fraction equation, the continuity and momentum conservation equations, and can be written as follows:

1) The volume fraction equation

$$\alpha_o + \alpha_w = 1 \tag{1}$$

2) The continuity equation

$$\frac{\partial \rho}{\mathrm{dt}} + \nabla \cdot \left(\rho \vec{v}\right) = 0 \tag{2}$$

3) The momentum conservation equation

$$\frac{\partial \left(\rho \vec{v}\right)}{\mathrm{dt}} + \nabla \cdot \left(\rho \vec{v} \vec{v}\right) = \tag{3}$$

$$-\nabla \rho + \nabla \cdot \left[\mu \left(\nabla \vec{v} + \nabla \vec{v}^{\mathrm{T}}\right)\right] + \rho \vec{g} + \vec{F}$$

where, α_o , α_w are the phase fraction of the oil phase, and water phase respectively. ρ, $\vec{v}$, and t are density, velocity, and time respectively. $\rho = \alpha_o\rho_o + \alpha_w\rho_w$, ρ_o, ρ_w are oil and water density respectively. p, g, μ, and F are pressure inside pipe, gravity acceleration, viscosity of the fluid and body force acting on the system respectively. $\mu = \alpha_o\mu_o + \alpha_w\mu_w$, μ_o, μ_w are oil and water viscosity respectively.

In this work, the mixture Reynolds number range (Re_m = 3566~10652) exceeds the turbulent critical Reynolds number, so the flow is turbulent, and the standard k-ε model is applied, which the turbulent kinetic energy (k) and viscous dissipation rate (ε) are computed and used to obtain the turbulent viscosity in the flow field [1].

4) The turbulent equations

$$\frac{\partial(\rho k)}{\partial t} + \nabla\cdot(\rho k\vec{v}) = \nabla(\frac{\mu_t}{\sigma_\varepsilon}\nabla k) + 2\mu_t E_{ij}E_{ij} - \rho\varepsilon \quad (4)$$

$$\frac{\partial(\rho\varepsilon)}{\partial t} + \nabla\cdot(\rho\varepsilon\vec{v}) = \nabla(\frac{\mu_t}{\sigma_\varepsilon}\nabla\varepsilon) + C_{1\varepsilon}\frac{\varepsilon}{k} + 2\mu_t E_{ij}E_{ij} - C_{2\varepsilon}\rho \quad (5)$$

where k, μ_t, ε are the turbulent kinetic energy, dissipation rate, and eddy viscosity respectively.

μ_t is defined as

$$\mu_t = C_\mu\rho\frac{k^2}{\varepsilon} \quad (6)$$

E_{ij} is defined as

$$E_{ij} = \frac{1}{2}\left(\frac{\partial v_i}{\partial x_j} + \frac{\partial v_j}{\partial x_i}\right) \quad (7)$$

The constants are: C_μ = 0.09, σ_k =1,σ_ε =1.3, $C_{1\varepsilon}$=1.44, $C_{2\varepsilon}$=1.92.

Surface tension and wall adhesion

The VOF model includes the impact of surface tension along with the interface of two phases. In this case, the continuum surface force (CSF) [1, 16, 28] is used as the surface tension model, and it is defined as the following form:

$$F = \sigma_f\frac{\rho\kappa_t\nabla\alpha_o}{\frac{1}{2}(\rho_o + \rho_w)} \quad (8)$$

where σ_f is the surface tension coefficient; ρ is the volume averaged density; κ_t is curvature and defined as [27].

$$\kappa_t = -\nabla\frac{\nabla\alpha_o}{|\nabla\alpha_o|} \quad (9)$$

Simulation model and settings

Simulation model

In order to investigate core annular flow inside the ball valve, the inner flow path is built into a three-dimensional model as a computational zone and is shown in Fig. 1. Two pipes of diameter 0.02m are in two ends of the valve, the ball radius of the valve is 0.013m, and its initial open rate is 15%. For obtaining detailed flow parameters, six sections (II is through the ball center, and the distance of between of I (or III) and II is 0.06m, X_I=-0.06, X_{II}=0, X_{III}=0.06, X_{IV}=0.12, X_V=0.18, X_{VI}=0.24) in computational zone are selected as study object. For establishing the core annular flow, co-axial entry of both the fluids with lube oil (ρ_o = 960 kg/m^3 and μ_o = 0.22 Pa.s [25]) at the center, and water (ρ_w = 998.2 kg/m^3 and μ_w = 0.001003 Pa.s) at the annular area has been considered as shown in Fig. 1. In this figure, the blue color indicates the water, and the red color indicates the oil phase.

This simulation is performed by employing the CFD system ANSYS Fluent 17 [29]. VOF model is selected, and the flow is inside of the pipe and valve, so the VOF sub model (the open channel and the open channel wave BC) is not used. The gravity effect is applied to the negative Y direction. And the explicit formulation is used for VOF method, the implicit body force is used for body force formulation. The Fnite Volume Method (FVM) is used to discretize the governing equations. After discretization, the segregated solver is used to solve these equations. The fluids are assumed as immiscible liquid pair, constant liquid properties and co-axial entry of the liquids. The calculation has been conducted for unsteady flow to analyze the initial development of oil-water flow [17].

Boundary condition

(1) Inlet boundary condition. The oil velocity is given at the center zone and water velocity at the annular zone. The velocity profile is assumed to uniform, and the initial conditions are:

At $0 \le r \le 0.013$ m, $v_x = v_{oil}$, the turbulent intensity is set as 5%, and hydraulic diameter is set as 0.014m;

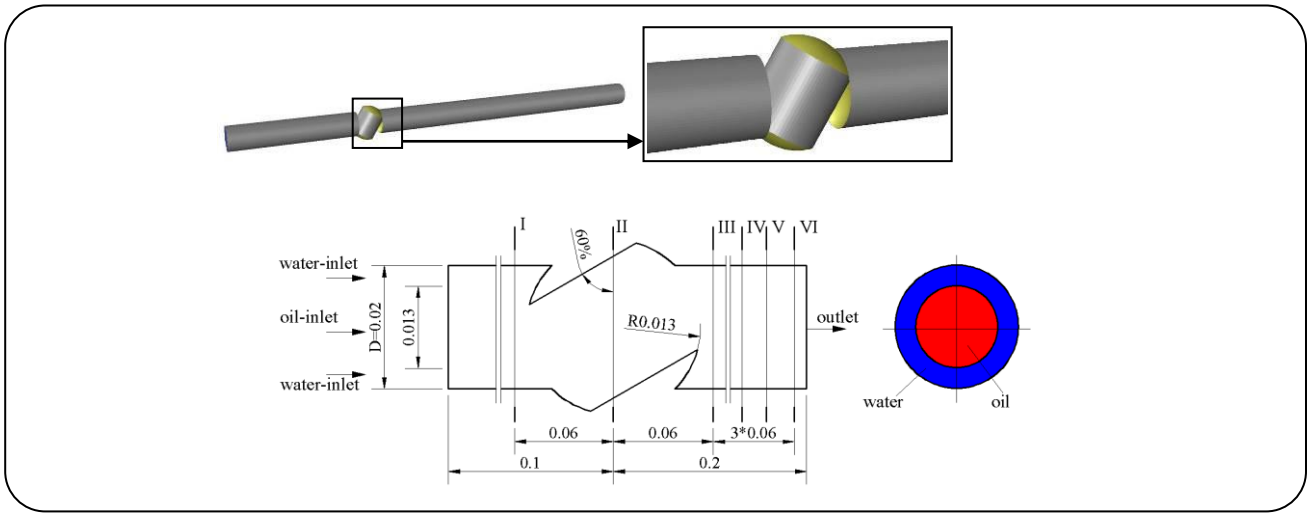

Fig. 1: The model geometry.

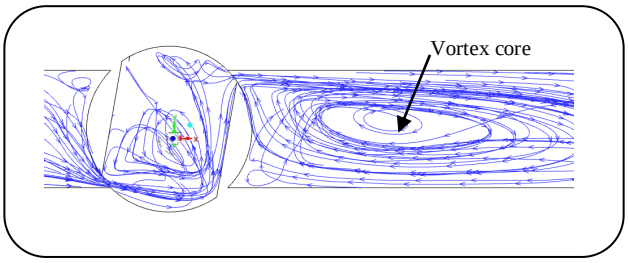

Fig. 2: The position of the vortex core.

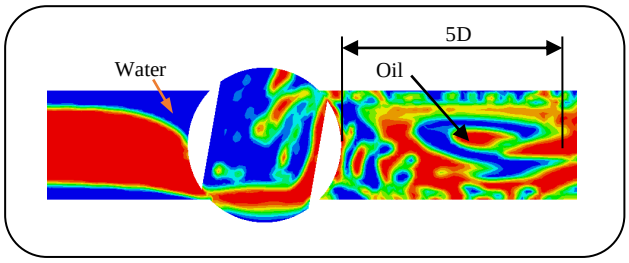

Fig. 3: The aggregation rate of the oil phase.

At $0.013 \le r \le 0.02$ m, $\nu_x = \nu_{water}$, the turbulent intensity is set as 5%, and the hydraulic diameter is set as 0.444m.

(2) Wall boundary conditions. The wall of the valve and pipe is a stationary boundary with no-slip and no penetration.

(3) Outlet boundary condition. The downstream outlet of pipe is set as a pressure outlet boundary, the turbulent intensity is set as 5% and the hydraulic diameter is set as 0.02m.

The evaluation parameters

In this work, the influence of the vortex in the computational zone on the interface of oil and water will be discussed, so the evaluation parameters should be defined.

(1) The position of vortex core x_{vc}, y_{vc}, z_{vc}, is shown in Fig. 2, a vortex is a region in a fluid in which the flow is rotating around an axis line. Its vortex core position may impact the oil-water core annular flow, and is defined as its coordinates value (e.g. X location for x_{vc}), and the coordinate origin is in the center of the valve.

(2) The aggregation rate of the oil phase, the oil-water core annular flow does not wish to be interrupted, so the oil core can keep aggregation is helpful to the heavy oil transportation. In this work, the aggregation rate of oil phase is used to evaluate the degree of oil aggregation. For this, the aggregation rate is the ratio of ideal oil phase zone number (is equal to 1) to the real oil phase zone number (n_0, the red zone in Fig. 3) in range of 5D behind of valve. The greater the aggregation rate, the less the oil core is scattered.

$$\eta = \frac{1}{n_o} \tag{10}$$

The meshed model

The computational domain is meshed by using software ANSYS Workbench. The grid model is depicted in Fig. 4. There are 270333 hexahedral cells and 292185 nodes. The grid independence test has been done and sample results are shown in Fig. 5. The figure confirms that α_o does not vary much when cells number is decreased from 401235 to 102514, and all results

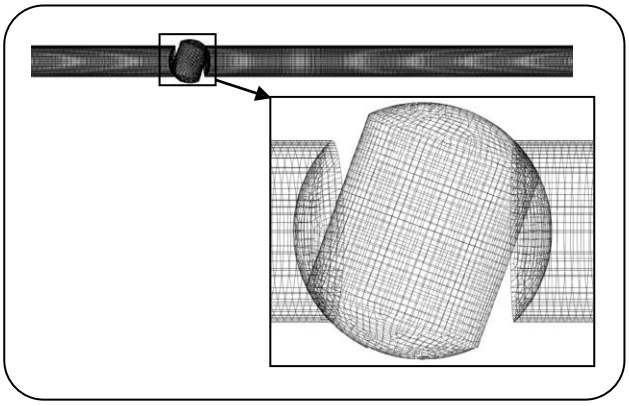

Fig. 4: The meshed geometry.

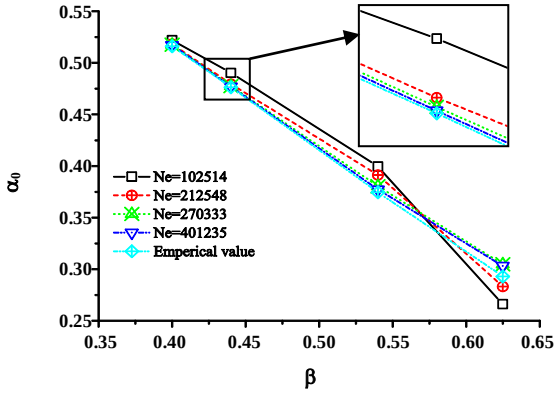

Fig. 5: Effect of elements numbers; v_{so}=0.53-1.29 m/s and v_{sw}=0.57-1.41 m/s

coincide with the empirical value well, the empirical formula is $\alpha_o = 1-\beta\left[1+0.35(1-\beta)\right]$, Where β is the inlet volume fraction of water [16].

Validation

For validating this simulation, the results are compared with the experimental data, the experiment of oil water core annular flow through the ball valve is conducted. The complete experimental set-up is shown in Fig. 6, which includes pipes, oil bump, water bump, annular flow nozzle, the counterbalance valve, rotameter, turbine flow-meter, pressure transducer, the ball valve, and so on. The oil and water property and pipe internal diameter are the same as the numerical simulation. For this work, v_{so} is varied from 0.53 to 1.29 m/s, and v_{sw} is varied from 0.57 to 1.41 m/s, that is, V1: v_{so1} = 0.53, v_{sw1} = 0.57, V2: v_{so2} = 0.91, v_{sw2} = 0.99, V3: v_{so3} = 1.29, v_{sw3} = 1.41. The simulation results of pressure loss between two ends of valve ($\Delta p = p_I - p_{II}$) are compared with those of experimental data is shown in Fig. 7, it is obvious that the numerical results are in agreement with the experimental data.

RESULTS AND DISCUSSION

After compared with experiments, the models are used to analyze the flow status and its parameters of core annular flow through the ball valve. In the following section, the developments of annular flow, flow parameters in the computational zone, the variation tendency of vertex location and oil aggregation rate are discussed.

The development of the core annular flow through the ball valve

The contours of oil volume fraction at difference time instants are shown in Fig. 8 (the cross-section location is indicated in Fig. 1). The red color indicates the oil while blue indicates the water. In the beginning, the computational zone is full of water phase and the oil phase gradually flows in, then the core annular flow is gradually formed with time in the front of the valve, but the shape of oil core changes when it passed through the valve center, in the little valve open rate, the oil phase is disturbed, and don't keep together.

When the open rate of valve increases, the oil-water core annular flow is disturbed lightly, is shown in Fig. 9. Compared Figs. 8 and 9, it is obvious that the core annular flow forming process inside the valve is influenced by the open rate.

Flow parameter in the computational zone

The flow parameters include the total pressure, velocity, streamline, turbulence kinetic energy, and so on. Fig. 10 depicts the total pressure contour, velocity vector, streamline, and turbulence kinetic energy for oil-water through the ball valve at v_{so}=0.53m/s and v_{sw}=0.57m/s, and the valve open rate is 60%, the time is 0.05s.

Fig. 10a depicts the pressure contour, and the total pressure is gradually decreasing from inlet to outlet. Because blocked by the valve, the total pressure at the inlet is greater than that at outlet. Fig. 10b describes the velocity vector distribution, for the radial direction, its velocity is higher at the center and gradually decreases to zero at the wall.

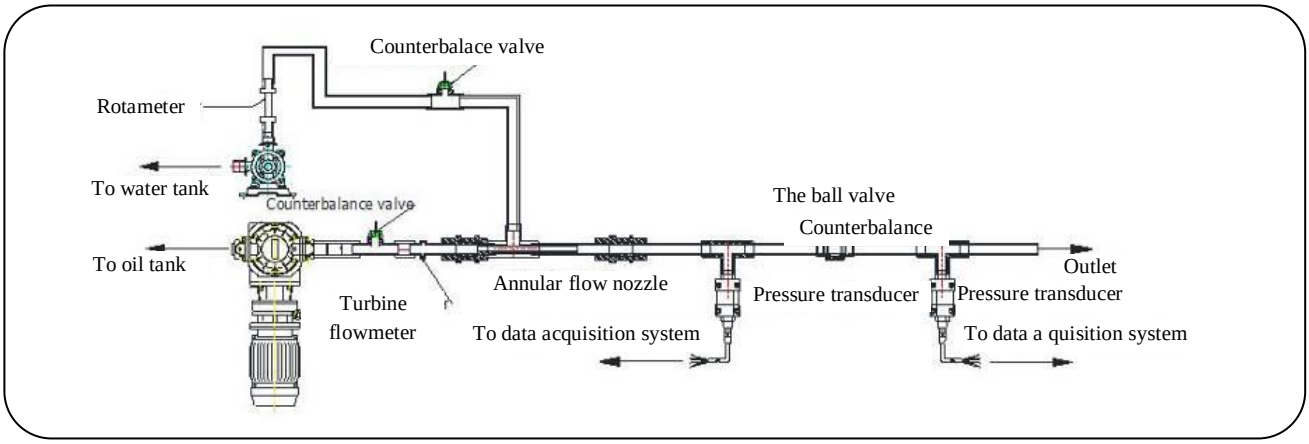

Fig.6: Schematic diagram of the oil-water test system.

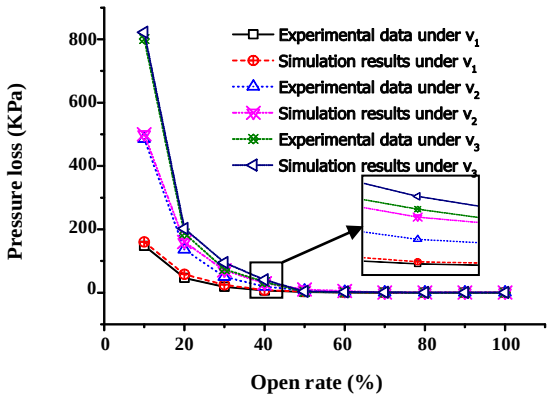

Fig. 7: Comparison of simulation results and experimental data; v_{so}=0.53-1.29 m/s and v_{sw}=0.57-1.41 m/s.

For flow direction, the velocity increases when the core annular flow across the valve due to the flow area variation. The streamline indicates that vortex is developing behind the valve, is shown in Fig. 10c. Owing to the influence of sharply changing area of the flow path, the fluids are jetted behind of the valve, and vortex is formed. Fig. 10d represents the contours of turbulence kinetic energy, the place with max kinetic energy is the place of vortex occurring.

The valve open rate influences the flow parameters too, is shown in Fig. 11.

Fig. 11a describes the variation of total pressure with increasing the valve open rate at six different axial locations of the pipe. The total pressure decreases sharply in section I and II, and increases lightly in the other section, this is due to the path size change steeply. At same time, the pressure reduces gradually when the fluid flows to the outlet. Fig. 11b represents the variation of velocity magnitude with increasing the valve open rate. The velocity decreases sharply in section II and III, and varies little in the other section. Because the sectional area in front of them changes greater, and the flow velocity varies largely. Fig. 11c depicts the variation of turbulence kinetic energy with increasing the valve opening rate. Their developing tendency is similar to the variation of velocity curves. Fig. 11d shows the volume fraction variation of oil phase with increasing the valve open rate. In section I, there is not much change in oil volume fraction, and in the other sections, the oil volume fraction changes greater. This is owing to that the oil core is broken to scatter in all directions, and the distribution of oil is messy, without regularity.

In order to understand the effect of input water fraction (β) on core annular flow, the different input water fractions are set, and the results are presented in Table 1 (the valve open rate is 50%). With the increase of the water fraction of the phase, the aggregation rate of the oil phase increases and the pressure loss increases on the section behind of valve. As a result of the increase of the water fraction, the oil phase after the valve can be concentrated, and the flow can be prevented, lead to the pressure loss increase.

The vortex study

Subsequently, efforts have been done to analyze the vortex characteristics and its effect factors. From Fig. 12, there are vortexes inside of the valve and the behind of the valve. Along increasing the open rate, the location of vortex core behind of the valve changes from the center

Table 1: the effect of input water fraction on the oil aggregation rate and pressure loss.

Input water fraction β	Input oil fraction	Oil aggregation rate on the section III	Pressure loss between section I and III (KPa)
0.520	0.480	0.485	1.37
0.536	0.464	0.512	2.75
0.540	0.460	0.529	17.2

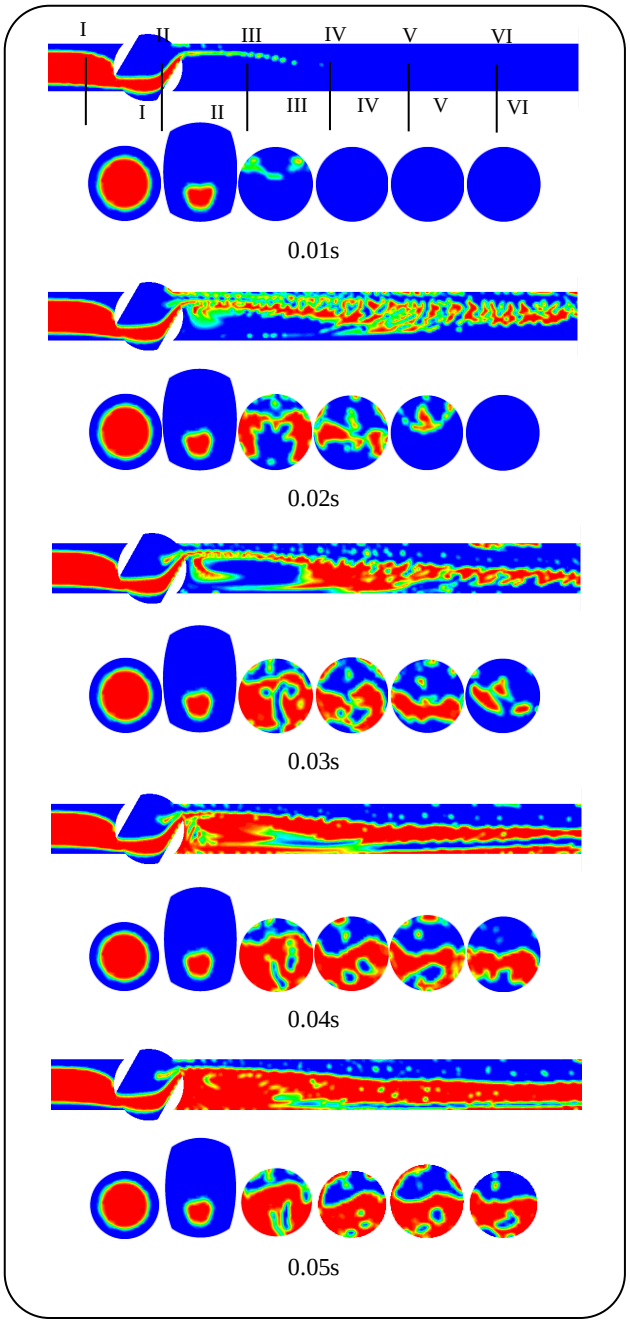

Fig. 8: Development of annular flow with time; v_{so}=0.53m/s and v_{sw}=0.57m/s, 30% open rate.

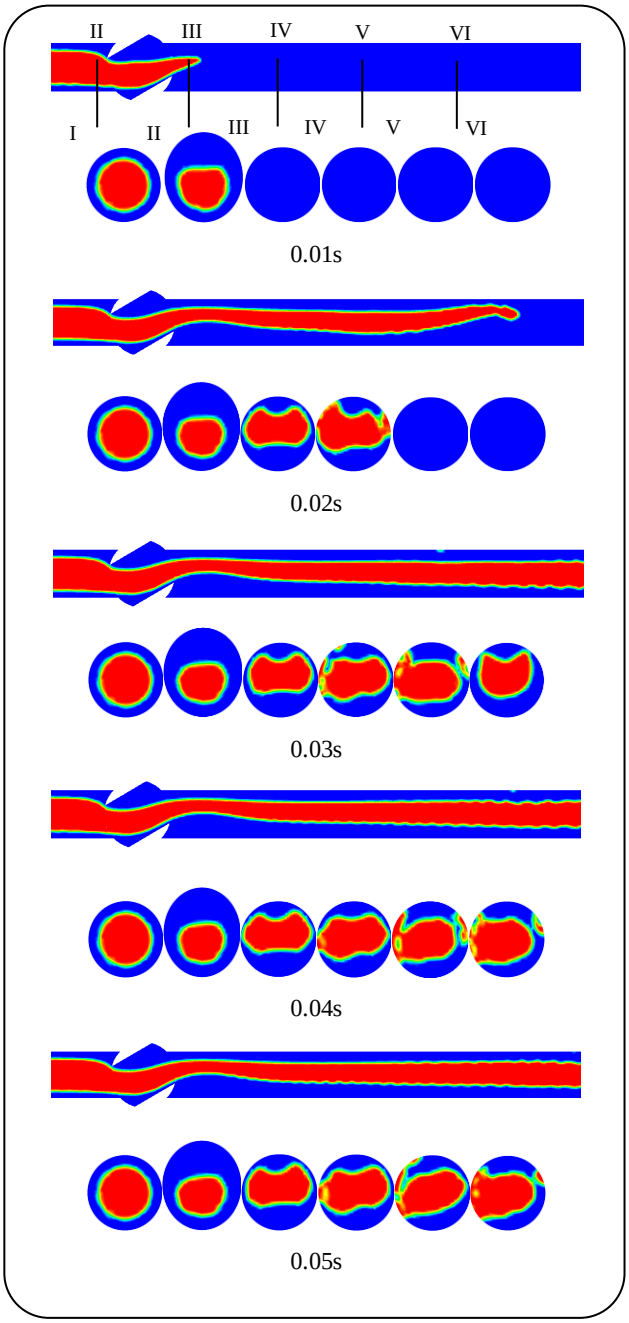

Fig. 9: Development of annular flow with time; v_{so}=0.53m/s and v_{sw}=0.57m/s, 60% open rate.

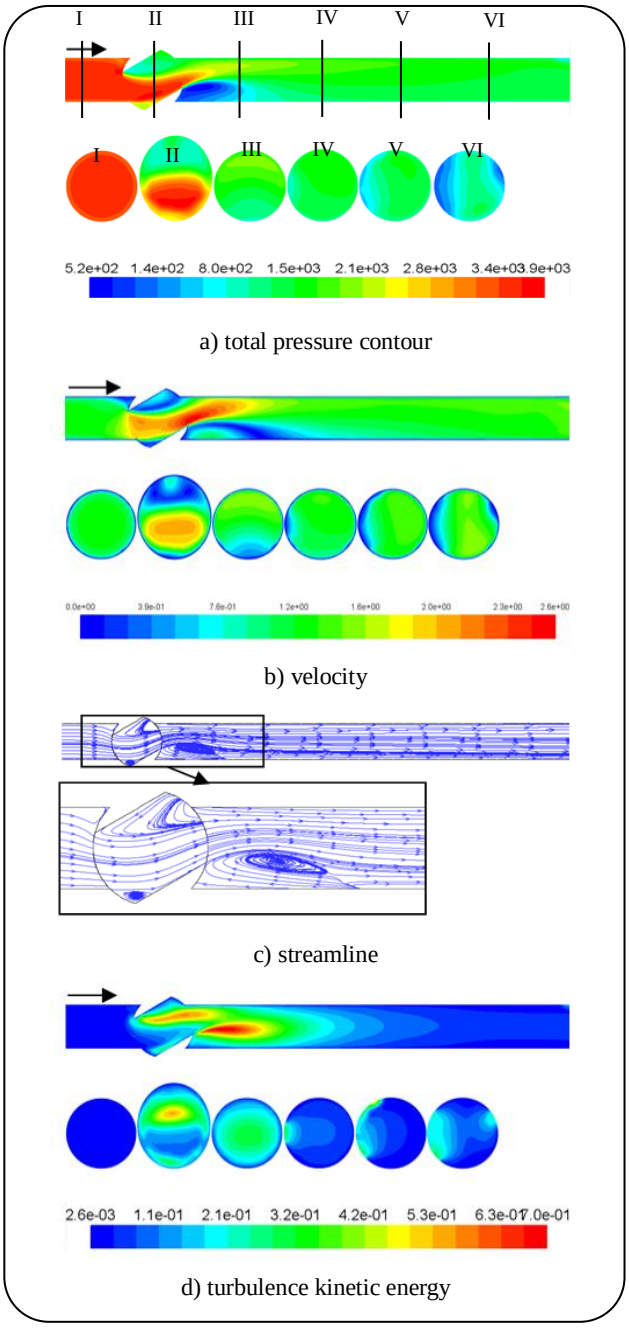

Fig. 10: Velocity contour (in m/s), velocity vector and total pressure contour (in Pa); at v_{so}=0.53m/s and v_{sw}=0.57m/s, 60% open rate, t=0.05s

of pipe to the lower left, and its scope is gradually narrowed. As the open rate is less than 30%, the flow state in the computational zone is disorder. This disorder flow leads to X location of vortex varied sharply.

Fig. 13 shows the coordinates value variation of vortex core location along with open rate and the input flow velocity. The vortex core location in the Z axis is the coordinates of the symmetric vortex in Y=0 plane. The vortex is symmetry for the plane with Z=0, so the positive z_{vc} (Z positive coordinate value) is only recorded, as no coordinates indicated vortex disappeared, x_{vc} (X coordinate value) is that the vortex is away from the valve center (Fig. 2). y_{vc} (Y coordinate value) is the location in Z=0 plane.

From Fig. 13, the x_{vc} decreases with an increasing open rate. When the open rate is 40%, the vortex is weak,and flow recovers smoothly. As the open rate reached 50%, the symmetry vortex disappeared, streamline in the export pipeline began to stabilize, but some little vortex are reforming. When the valve is opened to 70%, the vortex is very weak. The other direction coordinates (y_{vc} and z_{vc}) of the vortex are similar, they decrease with increasing of the open rate.

Effect of different input velocity on the vortex is conducted to study. As the input velocity increases, the change slope of the vortex position is greater. These results indicate that the core annular flow is stable and don't be disordered under condition of the high input velocity.

Fig.14 represents the vortex core locations vary with increasing of open rate under condition of different oil property. There are three oils, the lube oil, the crude oil, and the fuel oil. The lube oil property is noted previously, for the crude oil, ρ_{o2} = 925 kg/m^3 and and μ_{o2} = 0.5 Pa.s [30], for the fuel oil, ρ_{o3} = 960 kg/m^3 and μ_{o3} = 18 Pa.s [30]. From Fig. 14, they show similar variation, the vortex location coordinates decrease with the increasing of the open rate. At the same time, it can be seen that the oil property can affect the vortex location, the main factor is the viscosity of the oil, due to oil with low viscosity and good fluidity, velocity and direction of flow are relatively easy to be changed. To the high viscosity oil, the change of vortex core position is relatively slow.

The aggregation rate of the oil phase

A further attempt has been done to study the aggregation rate (η) of oil phase variation, and the effect of flow velocity and oil property on oil distribution. Fig. 15 depicts the aggregation rate of oil phase, as the valve opens from 10% to 60%, η is less than 1, in particularly, when the open rate is less than 30%, η is less than 0.1. This is because the small open rate, the smaller flow area

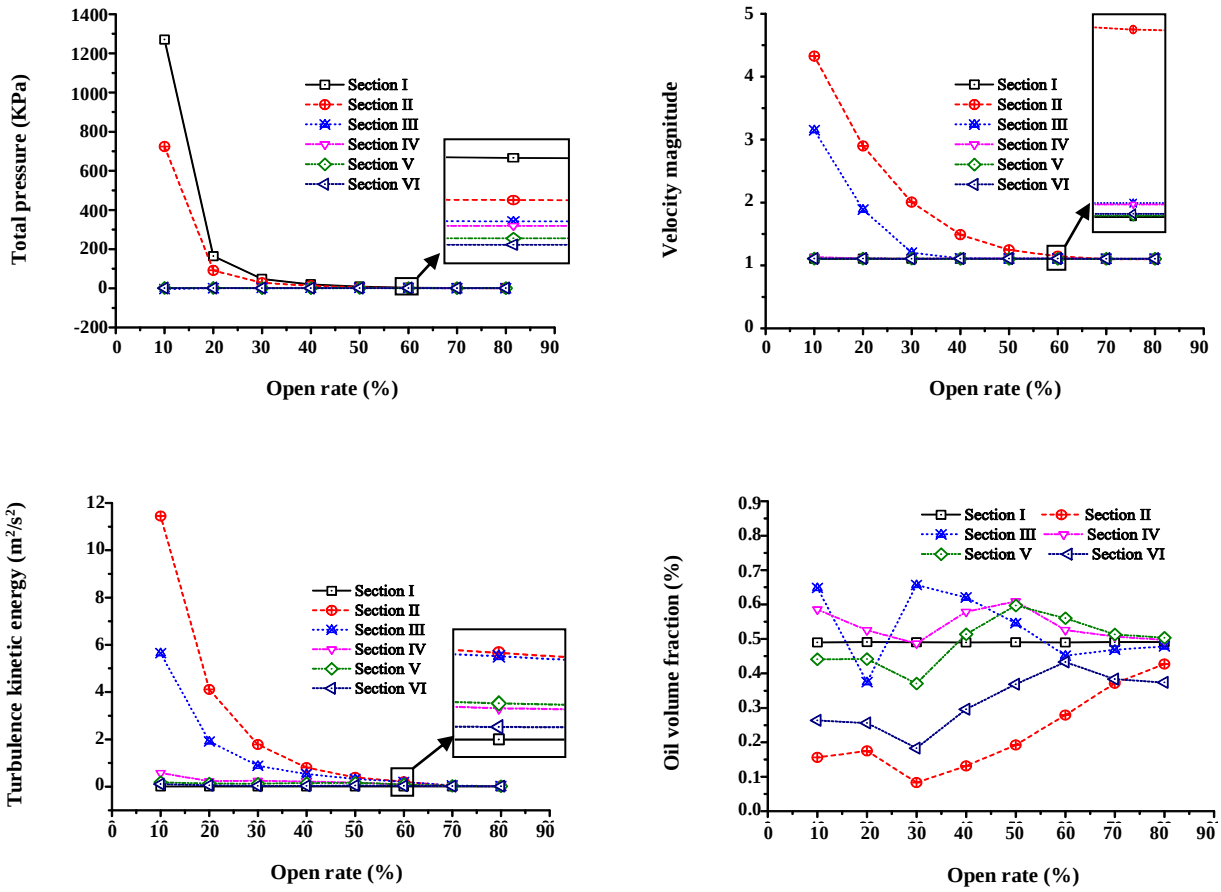

Fig. 11: Total pressure, velocity, turbulence kinetic energy, oil volume fraction in three sections at different opening rate; at v_{so}=0.53m/s and v_{sw}=0.57m/s, t=0.03s.

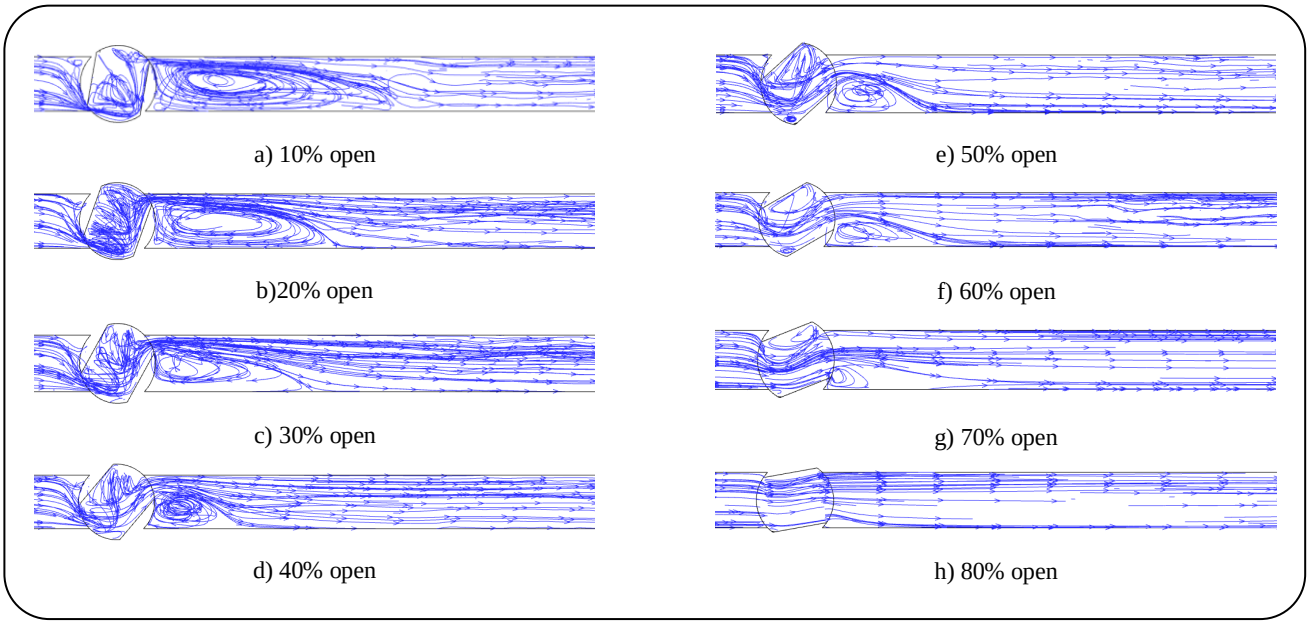

Fig.12: The vortex location variation along with open rate; at v_{so}=0.53m/s and v_{sw}=0.57m/s, t=0.03s.

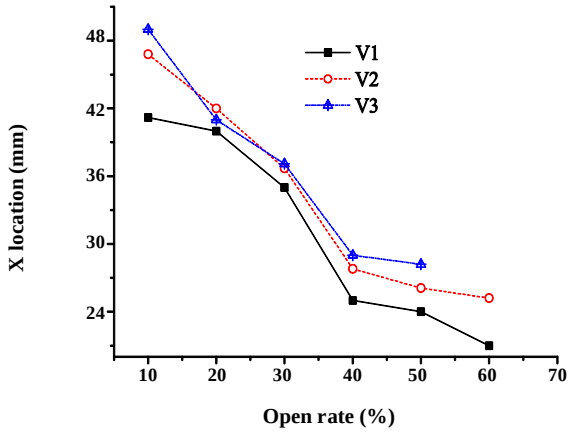

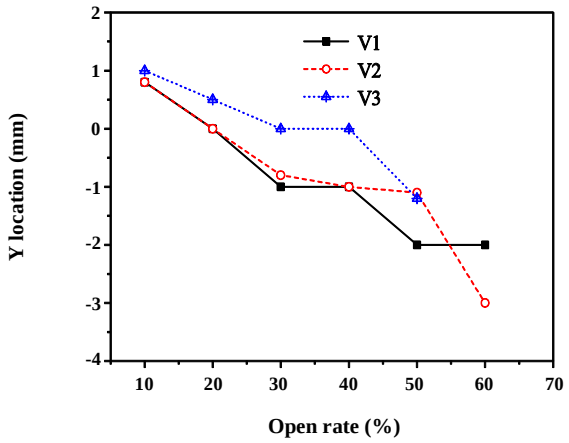

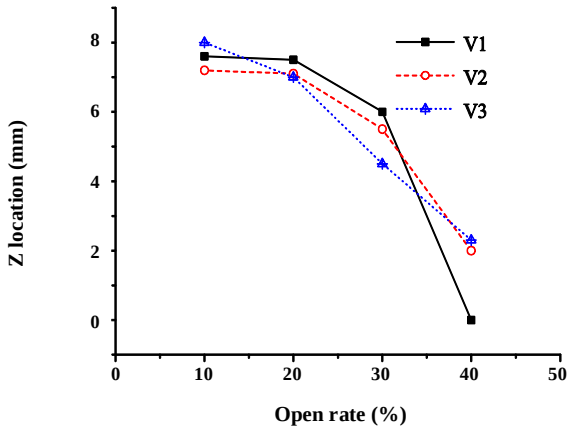

Fig. 13: The vortex core location at different opening rate.

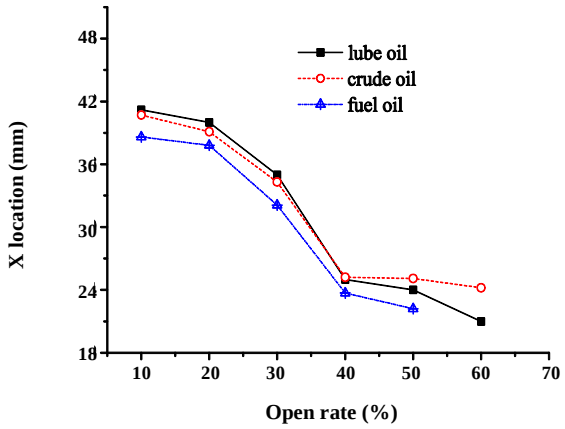

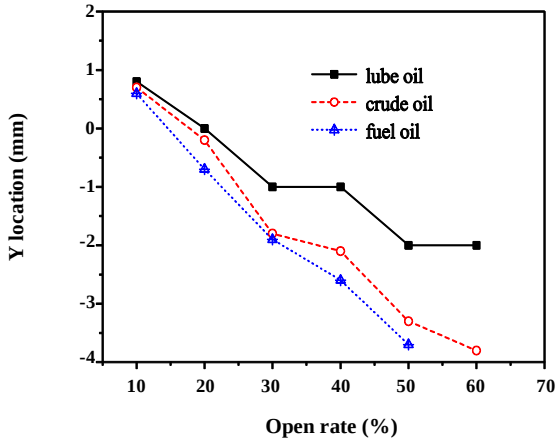

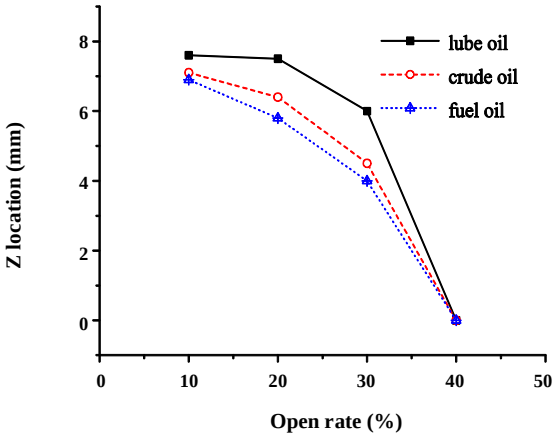

Fig. 14: The vortex core location at different oil properties.

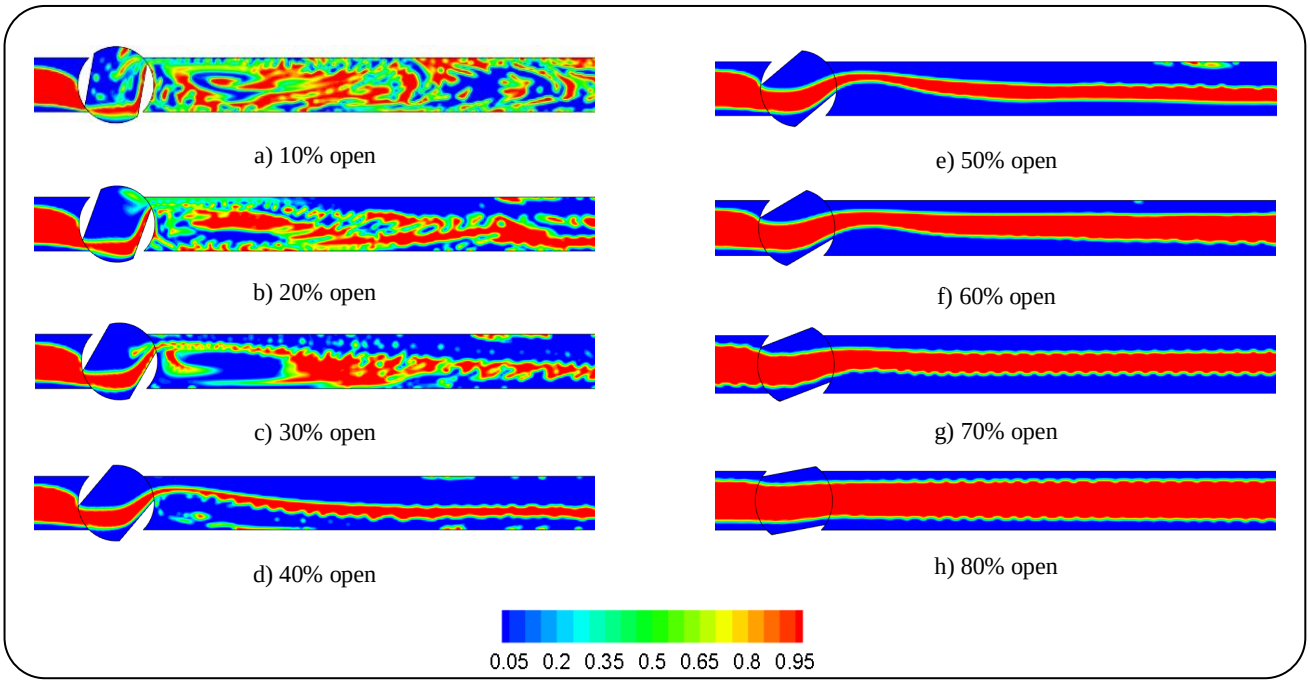

Fig. 15: aggregation rate of oil phase at different opening rate; at vso=0.53m/s and vsw=0.57m/s, t=0.03s.

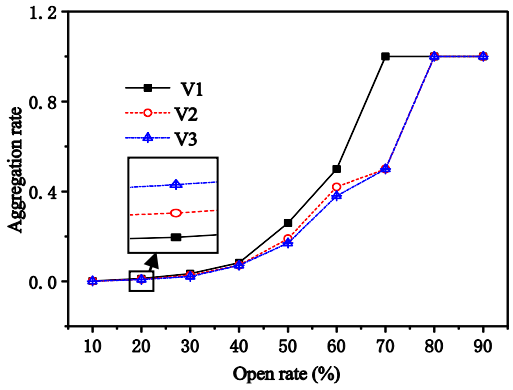

Fig. 16: The oil aggregation rate at different input velocity.

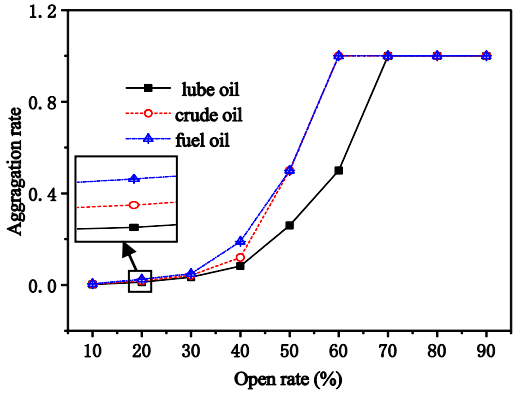

Fig. 17: The oil aggregation rate at different oil properties.

behind of the valve, and lead to the larger flow speed, the high speed fluid impact on the oil core, and the core annular flow is destroyed, the aggregation rate of The oil phase decreases. When the open rate increases to 70%, the aggregation rate of oil phase recovers to 1. From Fig. 15g and 15h, the axisymmetric bamboo waves are observed, these are agreed the experiments of *Bai et al.* [7].

Fig. 16 shows the effect of input velocity on the oil aggregation rate, it can be clearly seen that the input velocity increases, the oil aggregation rate decreases. Because the high speed flow influences the core annular flow, and the oil core is easily dispersed into many small oil droplets.

The effect of the oil property on the oil aggregation rate trend is depicted in Fig.17. From this figure, the oil with high viscosity has high oil aggregation after flow through the valve. This indicates the oil with high viscosity is not easily scattered. Bai et al. found that the high viscosity oil core may be assumed as a rigid solid which is not deformed by pressure forces in the water [31], this assume can explain the phenomenon of the high viscosity oil has high aggregation rate.

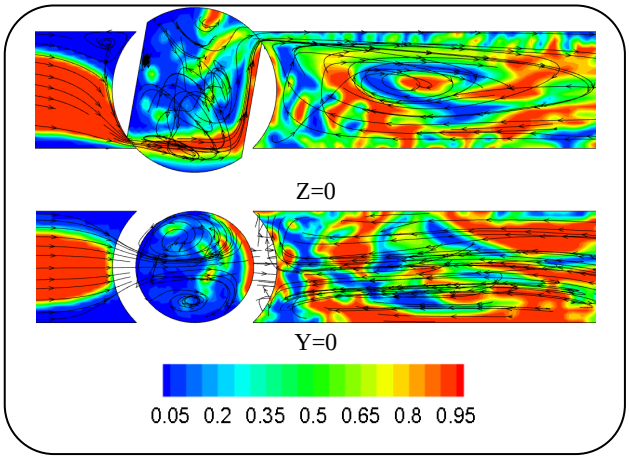

Fig.18: Relationship of vortex and oil aggregation rate at 10% open rate

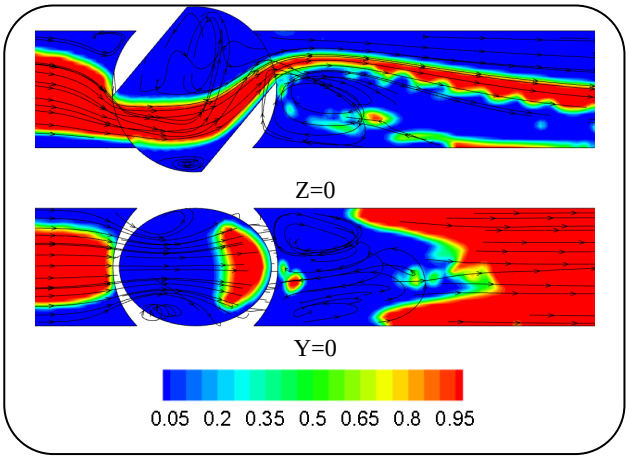

Fig.20: Relationship of vortex and oil aggregation rate at 40% open rate

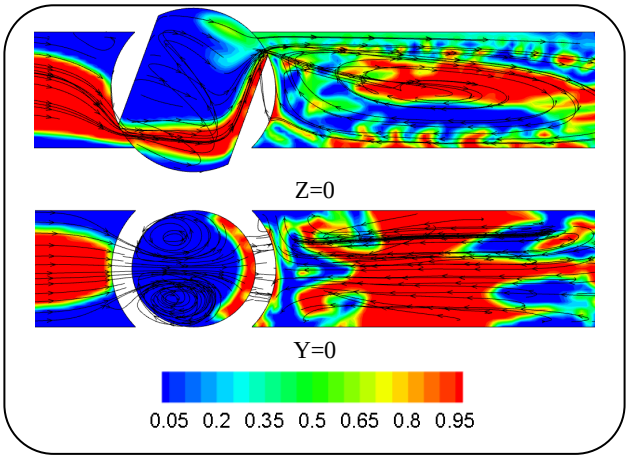

Fig.19: Relationship of vortex and oil aggregation rate at 20% open rate

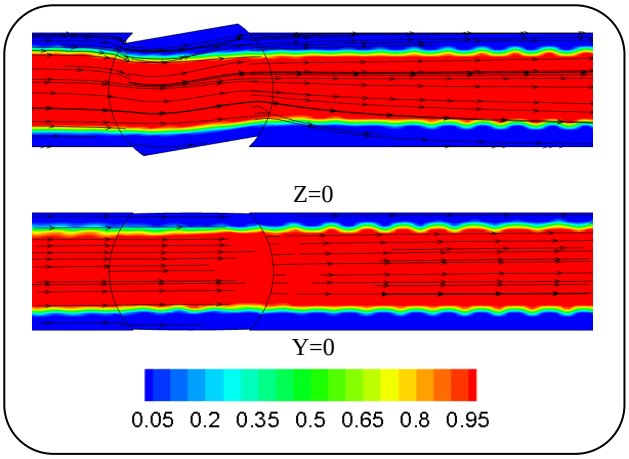

Fig.21: Relationship of vortex and oil aggregation rate at 80% open rate

The relationship between vortex and aggregation rate of oil phase

The relationship between the vortex and aggregation rate of the oil phase are also considered in this study.

From Fig. 18 to Fig.21, the streamline and the oil phase distribution are combined, and two sections are given. The vortex influences the oil phase distribution, only the streamline flow across through the oil core. Fig.18 shows the streamline flow across the location of the oil core, the oil is impacted to lots of small droplets in two sections under condition of 10% open rate.

Fig.19 and Fig.20 have similar phenomena, the jet flow across the oil zone, and the oil is scattered. But as the open rate is greater than 70% (Fig.21), the streamline is paralleled to the oil core, the oil is not destroyed.

The cavitation analysis

The absolute pressures of computation zone are compared among the difference open rates, and the absolute pressure with 10% open rate is minimum, 22766.2Pa, is greater than the saturated vapor pressure of water (2338.8Pa with the temperature of 20℃[32-33]), so the cavitation is not exist.

CONCLUSIONS

In the present work, the VOF model, $k-\varepsilon$ standard model, and CSF model are used to simulate the oil-water core annular flow through the ball valve. The calculated phase fraction agree well with the empirical correlation, and the pressure loss results are satisfied match with the experimental data. The influences of the valve open rate, input velocity, and oil property on the hydrodynamic and vortex and oil aggregation characteristics are discussed.

The simulation could bring insight into many information of oil-water core annular flow across the ball valve,

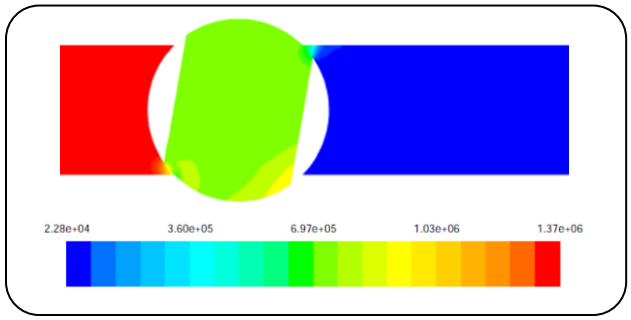

Fig.22: The absolute pressure of the computation zone at 10% open rate.

such as the development of oil-water flow, two phases' distribution, pressure distribution, turbulence kinetic energy, and velocity distributions. These results could provide references for optimizing the structure and operation parameters.

The oil-water core annular flow through the ball valve, under little open rate, the flow area varies steeply and leads to the complex flow state, the vortex occurs inside and behind the valve. As the vortex flow across the oil core, the oil is scattered and causes instability of annular flow.

From the simulations, the valve open rate, input velocity, and oil property have large influences on the vortex and oil aggregation characteristics. The vortex core coordinate values decrease and the aggregation rate increases with the increasing of the open rate. As the input velocity increases, the change slope of the vortex core position is greater, and the oil aggregation rate decreases, the oil with high viscosity has high oil aggregation after flow through the valve, and the variation of the vortex position is relatively slow.

Acknowledgements

The authors gratefully acknowledge research support from the Natural Science Foundation of Guangdong Province (2016A030313653) and the Science and Technology Plan of Guangzhou City (201607010291).

Received : Jul. 31, 2017 ; Accepted : Apr. 9, 2018

REFERENCES

[1] Jiang F., Wang Y.J., Ou J.J., Xiao Z.M., Numerical Simulation on Oil-Water Annular Flow Through the Π Bend, *Ind. Eng. Chem. Res.*, **53**: 8235-8244 (2014).

[2] Russell T.W.F., Charles M.E., The Effect of Less Viscous Liquid in the Laminar Flow of Two Immiscible Liquids, *Canad. J. Chem. Eng.*, **37**: 18-24 (1959).

[3] Charles M.E., Govier G.W., Hodgson G.W., The Horizontal Pipeline Flow of Equal Density of Oil–Water Mixtures, *Canad. J. Chem. Eng.*, **39**: 17-36 (1961).

[4] Arney M.S., Bai R., Guevara E., Joseph D.D., Liu K., Friction Factor and Hold up Studies for Lubricated Pipelining I. Experiments and Correlations, *Int. J. Multiphase Flow*, **19**: 1061-1067 (1993).

[5] Grassi B., Strazza D., Poesio P., Experimental Validation of Theoretical Models in Two-Phase High-Viscosity Ratio Liquid-Liquid Flows in Horizontal and Slightly Inclined Pipes, *Int. J. Multiphase Flow*, **34**: 950-965 (2008).

[6] Strazza D., Grassi B., Demori M., Ferrari V., Poesio P., Core-Annular Flow in Horizontal and Slightly Inclined Pipes: Existence, Pressure Drops, and Hold-Up, *Chem. Eng. Sci.*, **66**: 2853-2863 (2011).

[7] Bai R., Chen K., Joseph D.D., Lubricated Pipelining: Stability of Core-Annular Flow: Part 5. Experiments and Comparison with Theory, *J. Fluid Mech.*, **240**: 97-132 (1992).

[8] Gabryk K.M., Pietrzak M., Troniewski L., Study on Oil-Water Two-Phase Up Flow in Vertical Pipes, *J. Petrol. Sci. Eng.*, **117**: 28-36 (2014).

[9] Rodriguez O.M.H., Bannwart A.C., de Carvalho C.H.M., Pressure Loss in Core Annular Flow: Modeling, Experimental Investigation and Full Scale Experiments, *J. Petrol. Sci. Eng.*, **65**: 67-75 (2009).

[10] Bentwich M., Two-Phase Axial Laminar Flow in a Pipe with Naturally Curved Surface, *Chem. Eng. Sci.*, **31**: 71-76 (1976).

[11] Howard H.H., Daniel D.J., Lubricated Pipelining: Stability of Core-Annular Flow Part 2, *J. Fluid Mech.*, **205**: 323-356 (1989).

[12] Howard H.H., Neelesh P.F., Non-Axisymmetric Instability of Core-Annular Flow, *J. Fluid Mech.*, **290**: 213-224 (1995).

[13] Azizi S., Karimi H., Darvishi P., Flow Pattern and Oil Holdup Prediction in Vertical Oil–Water Two–Phase Flow Using Pressure Fluctuation Signal, *Iran. J. Chem. Chem. Eng. (IJCCE)*, **36**(2): 125-141 (2017).

[14] Li J., Renardy Y.Y., Direct Simulation of Unsteady Axisymmetric Core-Annular Flow with High Viscosity Ratio, *J. Fluid Mech.*, **391**: 123-149 (1999).

[15] Ooms G., Pourquie M.J.B.M., Beerens J.C., On the Levitation Force in Horizontal Core-Annular Flow with a Large Viscosity Ratio and Small Density Ratio, *Phys. Fluids*, **25**: 032102 (2013).

[16] Sumana G., Das G., Das, P.K., Simulation of Core Annular in Return Bends-A Comprehensive CFD Study, *Chem. Eng. Res. Des.*, **89**: 2244-2253 (2011).

[17] Jiang F., Wang Y.J., Ou J.J., Chen C.G., Numerical Simulation of Oil-Water Core Annular Flow in a U-Bend Based on the Eulerian Model, *Chem. Eng. Technol.*, **37**: 659-666 (2014).

[18] Jiang F., Long Y., Wang Y.J., Liu Z.Z., Chen C.G., Numerical Simulation of Non-Newtonian Core Annular Flow Through Rectangle Return Bends, *J. Appl. Fluid Mech.*, **9**: 431-441 (2016).

[19] Malgarinos I., Nikolopoulos N., Gavaises M., Coupling a Local Adaptive Grid Refinement Technique with an Interface Sharpening Scheme for the Simulation of Two-Phase Flow and Free-Surface Flows Using VOF Methodology, J. *Comput. Phys.*, **300**: 732-753 (2015).

[20] Laurmaa V., Picasso M., Steiner G., An Octree-Based Adaptive Semi-Lagrangian VOF Approach for Simulating the Displacement of Free Surfaces, *Comput. Fluids*, **131**: 190-204 (2016).

[21] Xu H., Guang Z.M., Qi Y.Y., Hydrodynamic Characterization and Optimization of Contra-Push Check Valve by Numerical Simulation, *Ann. Nucl. Energy*, **38**: 1427-1437 (2011).

[22] Posa A., Oresta P., Lippolis A., Analysis of a Directional Hydraulic Valve by a Direct Numerical Simulation Using an Immersed-Boundary Method, *Energy Convers. Manage.*, **65**: 497-506 (2013).

[23] Valdes J.R., Rodriguez J.M., Monge R., Pena J.C., Putz T., Numerical Simulation and Experimental Validation of the Cavitating Flow Through a Ball Check Valve, *Energy Convers. Manage.*, **78**: 776-786 (2014).

[24] Ghosh S., Das G., Das P.K., Simulation of core Annular Down Flow Through CFD -A Comprehensive Study, *Chem. Engin. Process.*, **49**: 1222-1228 (2010).

[25] Kaushik V.V.R., Ghosh S., Das G., Das P.K., CFD Simulation of Core Annular Flow Through Sudden Contraction and Expansion, *J. Petrol. Sci. Engin.*, **86-87**: 153-164 (2012).

[26] Habib A., Mousa M., Yousef N. K., A 3D Numerical Simulation of Mixed Convection of a Magnetic Nanofluid in the Presence of Non-Uniform Magnetic Field in a Vertical Tube using Two Phase Mixture Model, *J. Magn. Magn. Mater.*, **323**: 1963-1972 (2011).

[27] Reddy R. K., Joshi J. B., CFD Modeling of Solid–Liquid Fluidized Beds of Mono and Binary Particle Mixtures, *Chem. Engin. Sci.*, **64**: 3641-3658 (2009).

[28] Baltussen M.W., Kuipers J.A.M., Deen N.G., A Critical Comparison of Surface Tension Models for the Volume of Fluid Method, *Chem. Engin. Sci.*, **109**: 65-74 (2014).

[29] Ansys Inc., Fluent 17 User's Guide. USA, 2015.

[30] Bannwart A.C., Rodriguez O.M.H., de Carvalho C.H.M., Wang I.S., Vara R.M.O., Flow Patterns in Heavy Crude Oil-Water Flow, *J. Energ. Resour. Technol.*, **26**: 184-189 (2004).

[31] Bai R., Joseph D.D., Steady Flow and Interfacial Shape of a Highly Viscous Dispersed Phase, *Int. J. Multi. Flow*, **26**: 1469-1491 (2000).

[32] Mohammad T.S.T., Soran P., Morteza G., Numerical Study on the Effect of the Cavitation Phenomenon on the Characteristics of Fuel Spray, *Math. Comput. Model.*, **56**: 105-117 (2012).

[33] Tsukahara T., Maeda T., Hibara A., Mawatari K., Kitamori T., Direct Measurements of the Saturated Vapor Pressure of Water Confined in Extended Nanospaces using Capillary Evaporation Phenomena, *Rsc Adv.*, **2**: 3184-3186 (2012).